Similarity scaling of pressure fluctuation in turbulence

Yoshiyuki Tsuji[1] and Takashi Ishihara[2]
[1]*Department of Energy Engineering and Science, Nagoya University, Nagoya, Japan*
[2]*Department of Computational Science and Engineering, Nagoya University, Nagoya, Japan*
(Received 15 July 2002; published 20 August 2003)

Pressure fluctuation was measured in a turbulent jet using a condenser microphone and piezoresistive transducer. The power-law exponent and proportional constant of normalized pressure spectrum are discussed from the standpoint of Kolmogorov universal scaling. The clear power law with scaling exponent close to $-7/3$ was confirmed in the range of $600 \leqslant R_\lambda$. These Reynolds numbers are much larger than those in velocity fluctuation to achieve Kolmogorov scaling. The spectral constant is not universal but depends on Reynolds numbers. Measured pressure probability density functions are compared with direct numerical simulation.

DOI: 10.1103/PhysRevE.68.026309 PACS number(s): 47.27.Ak, 47.27.Jv

Static pressure fluctuation is a fundamental quantity contained in the dynamical equation of fluid motion, but it is the least understood quantity [1,2] due to the difficulty inherent in measuring this term by conventional equipment. There is an immense literature on the scaling properties of the velocity field [3], but despite the dynamical importance of the pressure relating to these scaling properties, little attention has been paid to the scaling properties of the pressure. Kolmogorov presented hypotheses for small-scale statistics based on the idea of local isotropy [1], which is restated by the relation

$$E_{pp}(k_1) = \rho^2 \langle \varepsilon \rangle^{3/4} \nu^{7/4} \phi_p(k_1 \eta), \tag{1}$$

for the case of pressure fluctuation, where ν is kinetic viscosity, $\langle \varepsilon \rangle$ is energy dissipation rate per unit mass on an average, and η is a typical length scale defined by $\eta \equiv (\nu^3/\langle \varepsilon \rangle)^{1/4}$. The wave number is defined by $k_1 \equiv 2\pi f/U$, where f is the time frequency and U the local mean velocity. ϕ_p is a nondimensional function. The pressure spectrum relates to the variance of pressure fluctuation

$$\langle [\tilde{p} - \langle p \rangle]^2 \rangle = \int_0^{+\infty} E_{pp}(k_1) dk_1, \tag{2}$$

where $\tilde{p}$ is the instantaneous fluctuation and $\langle p \rangle$ is its average. When the Reynolds number becomes large, according to Kolmogorov's idea, the spectrum exhibits a simpler form independent of kinetic viscosity:

$$E_{pp}(k_1) = K_p \rho^2 \langle \varepsilon \rangle^{4/3} k_1^{-7/3}. \tag{3}$$

The $-7/3$ power-law scaling was supported theoretically with various assumptions in the 1950s by Batchelor [4], Inoue [5], and Obukhoff and Yaglom [6]. George, Beuther, and Arndt [7] and Jones *et al.* [8] measured the pressure spectrum in the mixing layer of a round jet, and Elliott [9] and Albertson *et al.* [10] measured the pressure in the atmospheric boundary layer. But all these experiments were not enough to ascertain the power-law scaling exponent and the scaling form of Eq. (3). The relation was also investigated by analyzing the data of direct numerical simulation (abbreviated as DNS) of homogeneous isotropic turbulence [11–14]. However, the Reynolds number was too low to confirm the validity of the scaling form. At this stage, there is no consensus on the scaling exponent of the pressure spectrum and on the Kolmogorov similarity scaling.

In this paper, we measure the static pressure fluctuation in a fully developed turbulence and study how the spectral form varies depending on the Reynolds number. Especially, the spectral exponent and constant K_p are studied from the standpoint of Kolmogorov scaling. We compute the probability density functions and compare them with DNS in order to ascertain the qualitative accuracy.

The data were measured on the center line in a free jet. A small wind tunnel with a 40×40 mm^2 nozzle size and a large wind tunnel with a 400×700 mm^2 nozzle was operated in the velocity range of $5 \leqslant U_J \leqslant 15$. U_J m/s is the average velocity at the nozzle exit. The measured fluctuation velocity in the nozzle exit was less than 0.5%. On the center line downstream, $20 \leqslant x/D \leqslant 35$ ($D = 40$, 400 mm, the nozzle width), velocity and pressure fluctuation were measured for 15 min at a frequency of 10 kHz. The Reynolds numbers are in the range of $200 \leqslant R_\lambda \leqslant 1200$, where R_λ is the Taylor microscale Reynolds number. We used an *I* probe made of tungsten wire with a diameter of $\phi = 5\ \mu$m and a sensitive length of $\ell_s = 0.7$ mm. The probe was operated by a constant-temperature anemometer set at a distance of 2 mm from the pressure probe. Velocity and pressure fluctuations were measured at the same time.

The measurement of pressure fluctuation in the flow field was accomplished with a small piezoresistive transducer (Model XCS062, TEAC/KULITE) and a standard quarter-inch condenser microphone (Model 7017, Aco Co., Ltd). The transducer has a frequency response from dc up to 150 kHz with a dynamic range of 3.5×10^3 Pa. The maximum errors contained in linearity and hysteresis are 0.25%. A microphone is available for measuring the frequency of $20 \sim 70 \times 10^3$ Hz. The lower frequency is restricted due to its mechanical system. The dynamic range is $2 \times 10^{-2} \sim 3.2 \times 10^3$ Pa, so a very small amplitude can be measured. The probe is a standard Pitot-static tube measuring 1.0 mm in outside diameter and 0.1 mm in thickness as indicated in Fig. 1. Four static-pressure holes (0.4 mm in diameter) are spaced 90° apart and located at a distance of 22 tube diameters from the tip of the probe to minimize sensitivity to cross-flow error. The leeward end is terminated by the microphone or

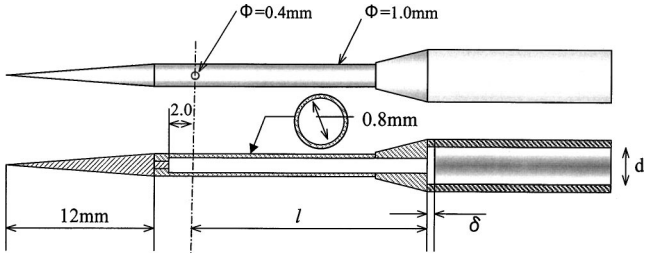

FIG. 1. Schematic view of static pressure probe. *d* is a diameter of sensor. It is 7.0 and 1.6 mm for microphone and transducer, respectively.

transducer. The sensor diameters are $d_T=1.6$ mm and $d_M=7.0$ mm for the transducer and microphone, respectively.

The transducer can detect the low-frequency pressure, but its amplitude cannot be small. The measurable amplitude was put at more than 10 Pa. The microphone can detect a very small amplitude, but low-frequency data cannot be obtained. This ability is the reverse to a transducer. Thus, a microphone is preferred for use with a low Reynolds-number flow because of its small amplitude but moderate-scale motions with a frequency of more than 20 Hz. The static pressure increases with the Reynolds number, and large-scale motions are generated accordingly. In this condition, a transducer is used instead of a microphone for measurement. We suppose that a microphone is available up to $R_\lambda \simeq 350$, but a transducer may be used beyond this Reynolds number.

The sensors were fitted with tubing as a pressure duct, and were inserted into the flow domain in such a way that the axis of the microphone (or the transducer) itself was aligned with the mean stream. We have preliminarily checked the angle between the pressure probe and the flow direction for its effect on the measured data. The error was less than 2.5% for $-15 \leqslant \theta \leqslant +15$. Statistical quantities such as spectrum and probability distribution function did not change significantly while θ was not so large.

The frequency response of the system is limited by the Helmholtz-resonator response of the tube and sensor cavity [7,16,17]. This frequency is calculated by

$$f_r = \frac{U_s}{2\pi}\sqrt{\frac{S}{\ell V}}, \tag{4}$$

where V is the cavity volume, ℓ is the tube length, U_s is the sound velocity, and S is the cross section (see also Fig. 1). Here, $V=\pi d^2\delta/4$ m^3 and $S=\pi(0.8\times10^{-3})^2/4$ m^2. The resonant frequency was computed to be 2.1 and 12.0 kHz for the microphone and transducer, respectively. Standing wave causes a small disturbance in pressure fluctuation. This frequency is given by $f_s=U_s/\lambda_s$, where $\lambda_s/4=\ell$. f_s is about 2.4 kHz for microphone and 4.6 kHz for transducer, respectively. The spatial resolution is estimated to be a few times tube diameter. Then, the corresponding frequency, $f_c=U_c/(n\times d)$, is taken into account in the measurements. Here, U_c is the local mean velocity, d is probe diameter, and n is to be from 2 to 5. f_s is of the order of 1.0 kHz at $U_c=5.0$ m/s. We set the low-pass filter by checking the frequency spectra. An example of measured pressure is plotted in Fig. 2. It is noted that the pressure fluctuation has occasionally large negative values. This negative spike is characteristic of pressure fluctuation.

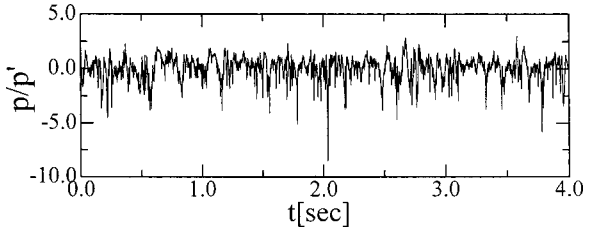

FIG. 2. Typical example of pressure fluctuation at $R_\lambda=1150$. Vertical axis is normalized by its standard deviation.

DNS of incompressible homogeneous turbulence was performed using periodic boundary conditions of periods of 2π in each of the three Cartesian coordinate directions. There are three different runs in which $R_\lambda=94(N=256^3)$, $164(N=512^3)$, and $283(N=1024^3)$. Here, N is the number of grid points. An almost statistically stationary state was achieved with an energy flux nearly equal to the energy dissipation rate $\langle\varepsilon\rangle$ in the case of $R_\lambda=283$. Detailed explanations on DNS are given in Ref. [18].

The probability density function (PDF) of pressure is negatively skewed. This was established in the early 1990s [19,20]. In Fig. 3 measured data (○ and +) are compared with DNS (solid line). Both Reynolds numbers are almost the same. The symbol ○ represents the microphone measurement and + represents the transducer, respectively. The microphone is available for low Reynolds number up to $R_\lambda \simeq 350$. The transducer, however, cannot be adopted below $R_\lambda \simeq 300$. PDF shifts to the positive side and its maximum peak locates a little away from $p=0$. There is a small qualitative difference between DNS and microphone around $|p/p'| \leqslant 1$, as shown in the inset. On the positive side, experimental values are slightly larger than those for the DNS. They are closer to the Gaussian profile (dotted line). On the negative side, $-6 \leqslant p/p' \leqslant 0$, PDFs agree with one another sufficiently.

Inertial scaling for pressure fluctuations is considered in terms of a one-dimensional spectrum $E_{pp}(k_1)$. George, Beuther, and Arndt derived the spectral form in the case of homogeneous constant-mean-shear flow [7]. They predicted that the pressure spectrum is generated by three distinct types of interaction in the velocity fields. In the inertial range the spectra associated with these three interaction modes exhibit $k_1^{-7/3}$, $k_1^{-9/3}$, and $k^{-11/3}$. George, Beuther, and Arndt [7] and Jones *et al.* [8] measured the pressure in the mixing layer of a round jet. They observed these different power-law exponents, but the scaling range was too narrow to determine the power-law exponent. Later, Kim and Antonia compared Jones's pressure spectrum with their DNS [22] and found that the inertial range property was not sufficiently resolved. Elliott [9] and Albertson *et al.* [10] measured the pressure in the atmospheric boundary layer. They reported $E_{pp} \propto k_1^{-1.7}$ and $k_1^{-3/2}$ relation, respectively. Albertson *et al.* concluded that this is due to the effect of large-scale motions in the flow. According to the recent DNS, E_{pp} is approximately proportional to $k_1^{-5/3}$, unlike Eq. (3), in the wave number

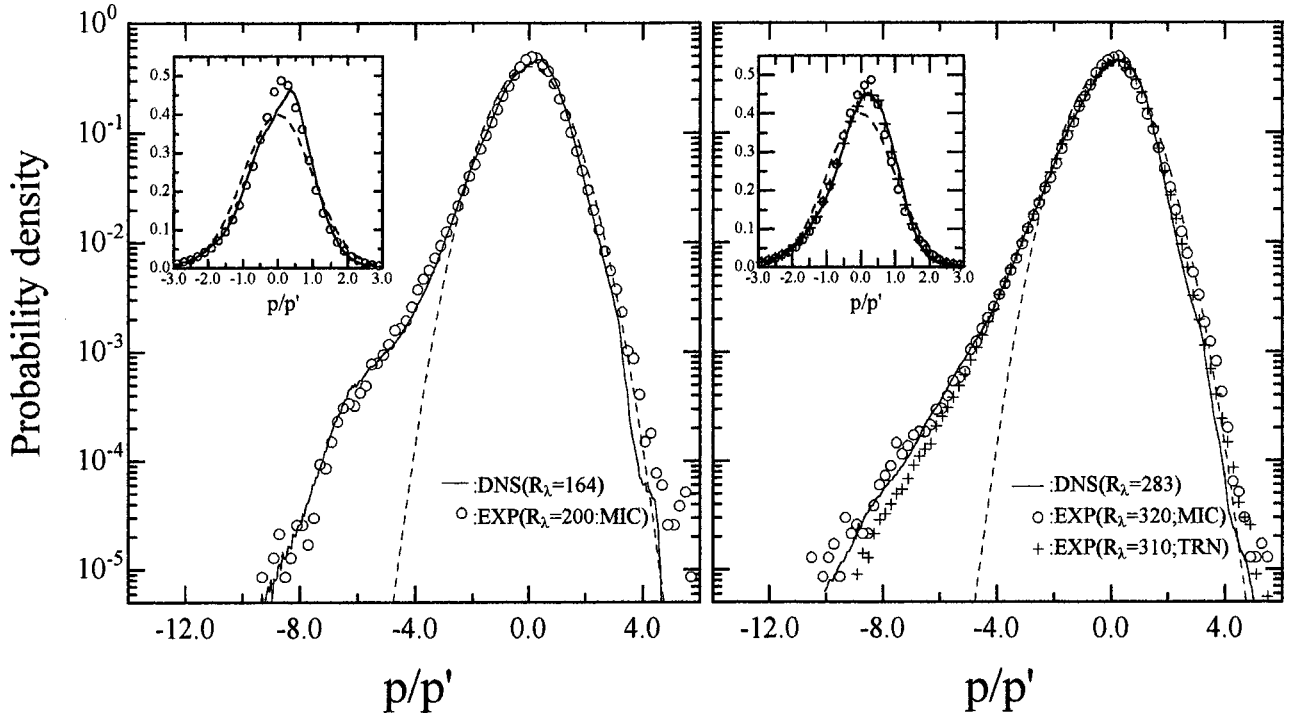

FIG. 3. PDF of measured pressure (symbols) are compared with DNS (solid lines). p' is a standard deviation of p. Insets show the core region $|p/p'| \leqslant 3.0$. Dotted line is Gaussian profile.

range where the energy spectrum exhibits close to $E_{uu} \propto k_1^{-5/3}$ [12–14]. In the high Reynolds number DNS, $R_\lambda \simeq 480$, exponent $-7/3$ was approximately observed [15]. Considering these previous studies, the power-law exponent of E_{pp} is not clarified at this stage and the validity of Eq. (3) remains to be proven.

A power-law exponent of pressure spectrum is systematically obtained by fitting the relation

$$E_{pp}(k_1) = K_p' \rho^2 \langle \varepsilon \rangle^{3/4} \nu^{7/4} (k_1 \eta)^{-\gamma_p}, \tag{5}$$

against the measured spectrum, while the normalized spectrum $E_{pp}/(k_1\eta)^{-\gamma_p}$ shows the broadest flat region. K_p' is a nondimensional quantity. In Fig. 4, the scaling exponents γ_p are plotted as a function of R_λ. They indeed depart from 7/3 in low Reynolds numbers. This trend is similar to the results of DNS [12–14]. But the exponents certainly approach 7/3 as the Reynolds number increases. This fact is consistent with the recent highest resolution DNS [24]. In this experiment, the $-7/3$ power-law scaling is confirmed for $600 \leqslant R_\lambda$.

The scaling exponent is about 1.95 at $R_\lambda \simeq 200$. It is slightly larger than the 5/3 observed in the DNS [12–14]. We suppose that this discrepancy is due to the different shape of spectral bump of DNS and that of the experiment. In Fig. 5, the pressure spectra are normalized in Kolmogorov scaling defined by Eq. (3). As the Reynolds number increases, there appears a flat region where we expect the inertial range. In the dissipation region, there is a small bump for $0.03 \leqslant k_1\eta$. It takes a maximum around $k_1\eta = 0.14$. However, in

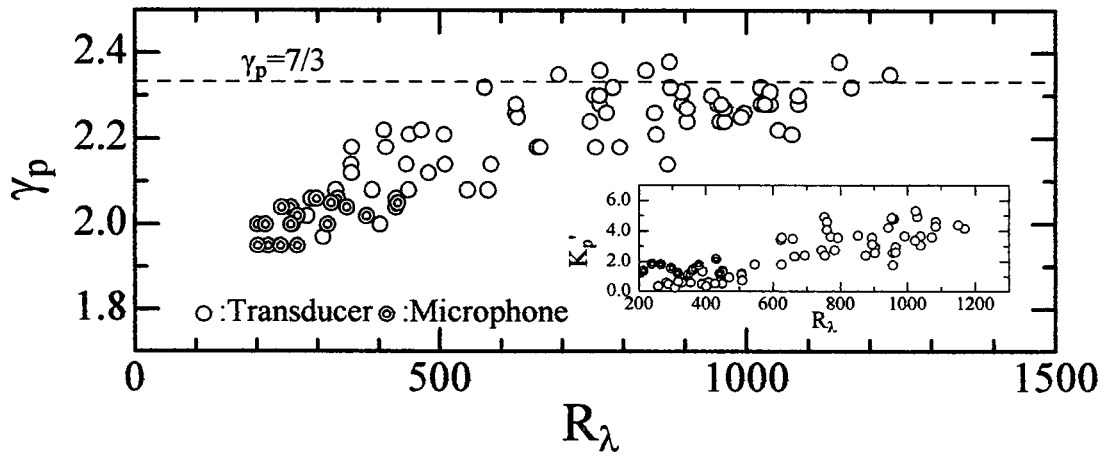

FIG. 4. Scaling exponent γ_p and constant K_p' defined by Eq. (6) are plotted as a function of Reynolds number.

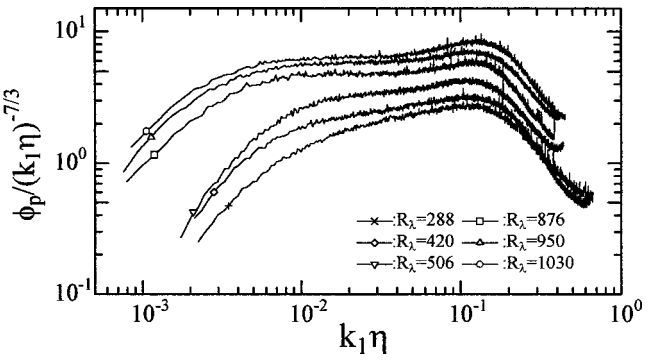

FIG. 5. Pressure spectra are normalized by Kolmogorov scaling defined by Eq. (4).

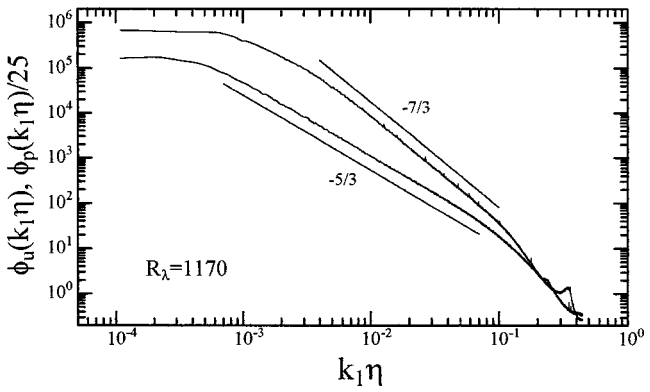

FIG. 6. Velocity and pressure spectra are normalized by Kolmogorov scales.

low Reynolds numbers it is difficult to distinguish between the inertial range and the bump region. Thus, the power-law exponent γ_p inevitably represents the slope of the beginning part of the bump. Gotoh and Fukayama reported that the $-5/3$ slope observed in DNS is due to the spectral bump around $k\eta \simeq 0.2$ [15]. Comparing the spectral bump in the experiment with that of DNS, the bump exists at almost the same location ($0.03 \leqslant k\eta$), but the DNS bump steeply increases and takes its maximum at $k\eta \simeq 0.2$. The maximum value, depending on the Reynolds number, is clearly larger than that in the experiment. It is noted that the high frequencies around the bump do not contribute to the negative tail of PDF. The negative tail consists of sharp pressure spikes as shown in Fig. 2.

There has been little discussion as to the value of a spectral constant. We had systematically obtained K_p' by means of Eq. (5), which are indicated in the inset of Fig. 4. K_p' is a increasing function of R_λ and it is 5.0 ± 1.0 at $R_\lambda \simeq 1000$. By fitting Eq. (3) against the measured spectrum within $0.02 \leqslant k_1\eta \leqslant 0.03$ at $R_\lambda = 420$ in Fig. 5, K_p is about 2.2. The flat region is very narrow, but this value is similar to that of Gotoh and Fukayama who reported $1.15 \leqslant K_p \leqslant 3.64$ at $R_\lambda = 480$. As the constant K_p is about 6.5 at $R_\lambda = 1030$, we conclude that the Reynolds number dependence of K_p is not negligible.

The exponent γ_p approaches 7/3 when R_λ is larger than 600. This is a significantly higher Reynolds number than needed for inertial scaling in velocity statistics. A typical example of velocity and pressure spectrum is indicated in Fig. 6. The pressure spectrum has a noticeably narrower scaling region than the velocity. This is consistent with the result that the higher Reynolds number is needed to realize a clear $-7/3$ power-law scaling. Hill and Wilczak derived an exact relation between the pressure structure function $\langle [\Delta p_r]^2 \rangle = \langle [p(x+r) - p(x)]^2 \rangle$ and the fourth-order velocity structure functions, $L(r) = \langle [\Delta u_r]^4 \rangle = \langle [u(x+r) - u(x)]^4 \rangle$, $T(r) = \langle [\Delta v_r]^4 \rangle = \langle [v(x+r) - v(x)]^4 \rangle$, and $M(r) = \langle [\Delta u_r]^2 [\Delta v_r]^2 \rangle$, under the assumptions of local isotropy [21]. Here, u is the stream-wise and v is the vertical velocity component. Hill and Boratav applied the relation to a low Reynolds number experiment and to a DNS with $R_\lambda = 82$, and concluded that the greater Reynolds number is necessary for the pressure structure function to achieve its inertial-range behavior [23]. This is consistent with our experiment.

Nelkin and Chen [25] computed the pressure structure function in terms of velocity structure functions $L(r)$, $T(r)$, and $M(r)$ obtained by an atmospheric experiment at $R_\lambda = 10\,000$. They concluded that $\langle [\Delta p_r]^2 \rangle$ is extremely sensitive to the small differences in scaling among the three quantities, $L(r)$, $T(r)$, and $M(r)$. The power-law exponents of pressure structure function $\zeta_2^{(p)}$ defined by $\langle [\Delta p_r]^n \rangle \propto r^{\zeta_n^{(p)}}$ was derived as $\zeta_2^{(p)} = 1.17$, or the spectral exponent is $\gamma_p = 2.17$. This value is close to the present result at $R_\lambda \simeq O(10^3)$ in Fig. 5.

We are grateful to Professor T. Gotoh, Professor K. R. Sreenivasan, and Professor Y. Kaneda for their valuable comments and advice on the draft version of this paper.

[1] A.S. Monin and A.M. Yaglom, *Statistical Fluid Mechanics* (MIT, Cambridge, MA, 1975), Vol. 2.
[2] M. Nelkin, Adv. Phys. **43**, 143 (1994).
[3] K.R. Sreenivasan and R.A. Antonia, Annu. Rev. Fluid Mech. **29**, 435 (1997).
[4] G.K. Batchelor, Proc. Cambridge Philos. Soc. **47**, 359 (1951).
[5] E. Inoue, Geophys. Mag. **23**, 1 (1951).
[6] A.M. Obukhoff and A.M. Yaglom, National Advisory Committe for Aeronautics, Technical Memorandum **1350**, 1 (1953).
[7] W.K. George, P.D. Beuther, and R.E.A. Arndt, J. Fluid Mech. **148**, 155 (1984).
[8] B.G. Jones, R.J. Adrian, C.K. Nithianandan, and H.P. Planchon, Jr., AIAA J. **17**, 449 (1979).
[9] J.A. Elliott, J. Fluid Mech. **53**, 351 (1972).
[10] J.D. Albertson, G.G. Katul, M.B. Parlange, and W.E. Eichinger, Phys. Fluids **10**, 1725 (1998).
[11] A. Pumir, Phys. Fluids **6**, 2071 (1994).
[12] T. Gotoh and R. Rogallo, J. Fluid Mech. **396**, 257 (1999).
[13] P. Vedula and P.K. Yeung, Phys. Fluids **11**, 1208 (1999).
[14] N. Cao, S. Chen, and G.D. Doolen, Phys. Fluids **11**, 2235

(1999).
[15] T. Gotoh and D. Fukayama, Phys. Rev. Lett. **86**, 3775 (2001).
[16] Y. Kobashi, J. Phys. Soc. Jpn. **12**, 533 (1957).
[17] Y. Shirahara and K. Toyoda, Japan Soc. Mech. Engineering **59**, 3381 (1993) (in Japanese).
[18] T. Ishihara and Y. Kaneda, in *Proceedings of the International Conference on Statistical Theories and Computational Approaches to Turbulence*, 2001, edited by Y. Kaneda and T. Gotoh (Springer, Tokyo, 2002), p. 178.
[19] M.E. Brachet, Fluid Dyn. Res. **8**, 1 (1991).
[20] S. Fauve, C. Laroche, and B. Castaing, J. Phys. II **3**, 271 (1993).
[21] R.J. Hill and J.M. Wilczak, J. Fluid Mech. **296**, 247 (1995).
[22] J. Kim and R.A. Antonia, J. Fluid Mech. **251**, 219 (1993).
[23] R.J. Hill and O.N. Boratav, Phys. Rev. E **56**, R2363 (1997).
[24] T. Ishihara, Y. Kaneda, M. Yokokawa, K. Itakura, and A. Uno, J. Phys. Soc. Jpn. **72**, 983 (2003).
[25] M. Nelkin and S. Chen, Phys. Fluids **10**, 2119 (1998).